

## Article

# Analysis of Extreme Rainfall Characteristics in 2022 and Projection of Extreme Rainfall Based on Climate Change Scenarios

Jang Hyun Sung <sup>1</sup>, Dong Ho Kang <sup>1</sup>, Young-Ho Seo <sup>1</sup> and Byung Sik Kim <sup>2,\*</sup>

<sup>1</sup> Department of Urban and Environmental Disaster Prevention Engineering, Kangwon National University, Samcheok-si 25913, Republic of Korea; jhsung@kangwon.ac.kr (J.H.S.); kdh@kangwon.ac.kr (D.H.K.); yhseo@kangwon.ac.kr (Y.-H.S.)

<sup>2</sup> Department of Artificial Intelligence & Software, Kangwon National University, Samcheok-si 25913, Republic of Korea

\* Correspondence: hydrokbs@kangwon.ac.kr; Tel.: +82-33-570-6819

**Abstract:** In this study, we analyzed the characteristics of the heavy rainfall events that occurred in Seoul in 2022 and compared them with the projections of the representative concentration pathway (RCP). The analysis results indicated that climate change is ongoing. In this era of climate crisis, based on the shared socioeconomic pathway (SSP) data, we projected the 20-year frequency rainfall for South Korea at intervals of 1 day/24 h. Our results indicate that the maximum rainfall (with a 24 h duration) will increase by ~18% in the second half of the 21st century, compared to the current maximum rainfall. Finally, we projected the intensity–duration–frequency (IDF) curve for the infrastructure design of Seoul. According to the projected IDF curve, across all durations, the rainfall intensity was the strongest in the early 21st century, indicating that at present, we are in the midst of a climate crisis. Thus, it is important to develop and implement effective urban and river flood management measures to mitigate the current effects of climate change. Notably, our study can serve as a reference for future studies on climate change and help policymakers and decision-makers develop relevant policies and mitigation strategies related to the effects of climate change.

**Keywords:** representative concentration pathway (RCP); climate change; shared socioeconomic pathway (SSP); intensity–duration–frequency (IDF) curve; Seoul; urban flood



**Citation:** Sung, J.H.; Kang, D.H.; Seo, Y.-H.; Kim, B.S. Analysis of Extreme Rainfall Characteristics in 2022 and Projection of Extreme Rainfall Based on Climate Change Scenarios. *Water* **2023**, *15*, 3986. <https://doi.org/10.3390/w15223986>

Academic Editor: Pavel Groisman

Received: 17 October 2023

Revised: 2 November 2023

Accepted: 12 November 2023

Published: 16 November 2023



**Copyright:** © 2023 by the authors. Licensee MDPI, Basel, Switzerland. This article is an open access article distributed under the terms and conditions of the Creative Commons Attribution (CC BY) license (<https://creativecommons.org/licenses/by/4.0/>).

## 1. Introduction

In the last 20–30 years, South Korea has experienced the effects of climate change several times, and several studies indicate that extreme climate-related events (different from before) are occurring around the world, owing to the abnormalities caused by climate changes. Compared to the consensus on the statistical non-stationarity of hydrometeorological processes caused by climate change (increased risk of more intense heavy rainfall than that observed historically), studies on the improvement of the design level, while considering the factors of statistical non-stationarity, are limited. In the case of Seoul, if climate change had been considered in the design of the inland drainage facility, the current damage would have been less. Indeed, an increase in the daily rainfall was confirmed in both the observations and climate models of the second half of the 20th century [1], with projected multi-decade increases in the rainfall extremes, especially in the short-duration rainfall extremes. Previous research reports substantial evidence of such events getting stronger [2]. Most hydrological infrastructure designs are based on rainfall intensity–duration–frequency (IDF) curves that provide extreme rainfall intensity (mm/h) values for various durations (from minutes to days) and return periods (year).

Floods are generally classified into four types: fluvial, pluvial, flash, and coastal floods. Among them, fluvial flood denotes the flooding of the river embankment due to a rise in the water level of the river; a pluvial flood is the inundation caused by saturation of the urban drainage system. In South Korea, fluvial floods are rare due to steady embankment

maintenance; however, urban floods have been occurring frequently, owing to the increase in short-duration heavy rainfall events ( $>80$  mm/day), e.g., the heavy rainfall events that occurred in Gangnam in South Korea in 2010, 2011, and 2022. As pluvial floods occur in densely populated areas, they can cause great damage. The damage can be aggravated, owing to the increasing population density in urban Seoul. The most concerning fact is that the concentration of population and assets in such cities is still increasing. Notably, as of 2021, in South Korea, approximately 92% of the total population (47.4 million of the total population of 51.64 million) lives in cities. In particular, the effects of climate change, e.g., the changes in the scale and frequency of extreme events, have been realized previously [3]. In this era of climate crisis, it is necessary to secure the sustainability of flood management in urban areas, where population and assets are concentrated.

Several previous studies have reported the non-stationarity of the extreme rainfall time series [4,5]; in these studies, extreme rainfall at the global and regional scales was considered to develop estimated exceedance probability curves, using a global circulation model (GCM). Ref. [6] observed that changes in the extreme rainfall values increased with the return period of the rainfall; however, the values increased with the decreasing duration of the rainfall. Thus, for the European region, on average, a 24 h rainfall event with a return period of 20 years increased by 18% by the end of the 21st century. The authors of [7] simulated the rainfall over North Korea; they concluded that the return period of 20 years for the reference period of 1980–2005 will increase to 21.1 years in 2011–2040, followed by a decrease to 16.2 years in 2041–2070 and 8.8 years in 2071–2100. GCM generally has a temporal resolution of more than 1 day, and sub-daily precipitation series are required to examine changes in the frequency and intensity of sub-daily rainfall events [8–11].

In accordance with the Representative Concentration Pathways (RCPs), the previous study projected an increase in the frequency of extreme rainfall events in South Korea throughout the 21st century. Concurrently, empirical evidence from observations in the early 21st century (2011–2040) substantiates the emergence of a climate crisis. Nevertheless, a quantitative assessment comparing these current observations with the climate crisis projected by RCPs in the early 21st century has not been undertaken. Therefore, the ongoing climate crisis was evaluated by comparing the current situation of precipitation that caused urban flooding in Seoul in 2022 with simulations of future climate change scenarios. The observations showed that the exceedance probability of sub-daily rainfall was significant. Nevertheless, in most cases, the projected changes in future extreme rainfall were based on daily rainfall data. To obtain the probability of rainfall by duration required for estimating the floods caused by extreme rainfall in the future, the GCM, which was based on the shared socioeconomic pathways (SSPs), was statistically refined to the observation-point scale, to project future climate change scenarios for each observation point. The obtained daily precipitation was then converted into the 24 h rainfall projection, and the IDF curve was constructed using the scaling-generalized extreme value (GEV) distribution model. Finally, we propose a non-structural measure to respond to similar flood events in the future.

## 2. Data and Method

### 2.1. Method

In this study, we analyzed the characteristics of the heavy rainfall that occurred in South Korea in 2022 (8–10 August 2022). The data of the series of extreme rainfall events pertaining to the period were collected, and the return period was estimated by fitting the maximum rainfall series for each duration to the GEV distribution model. The results were compared with the future forecast (2011–2040) developed through the representative concentration pathway (RCP) 8.5 scenario. In addition, to improve the sustainability of the infrastructure design of Seoul, we presented the IDF curve of future rainfall in Seoul through the scaling-GEV model, based on different SSP scenarios. First, the maximum daily and 24 h extreme rainfall were projected as a future climate change scenario, and the scaling characteristics were obtained from 1 h to 24 h of observation and expanded to the climate change scenario to project the future IDF curve for Seoul (Figure 1).

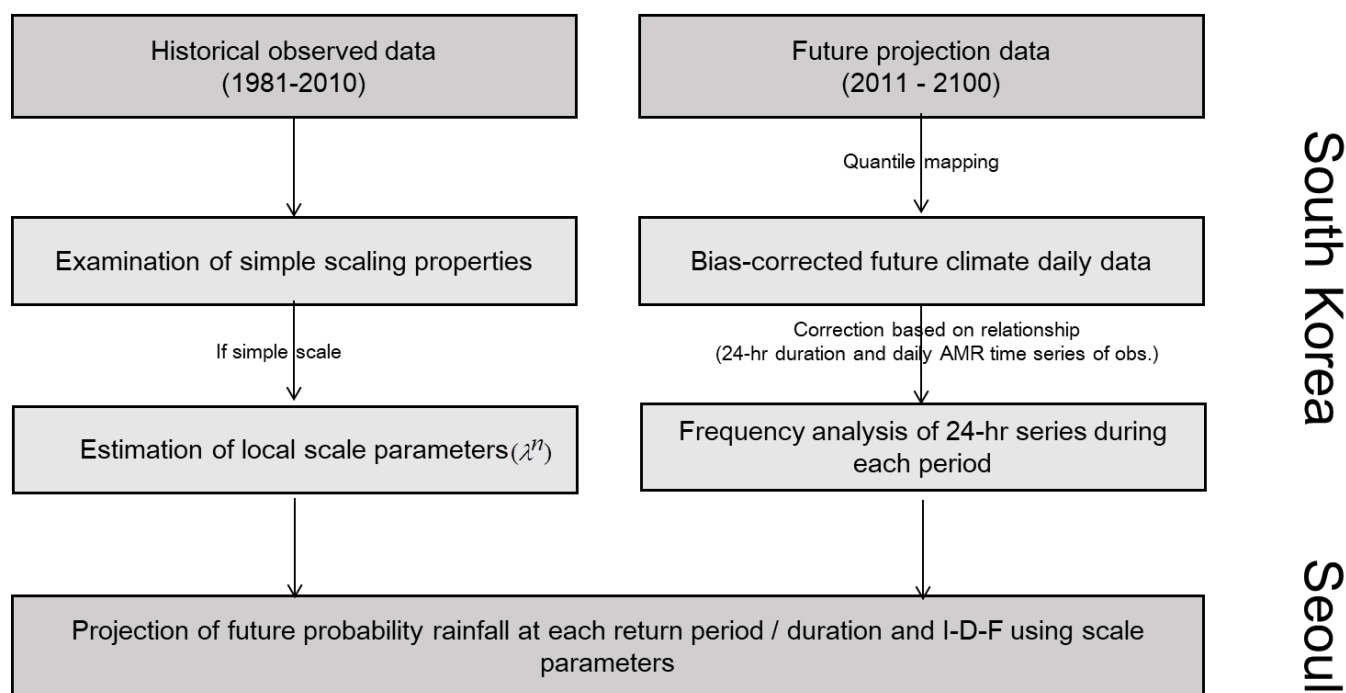


**Figure 1.** Flowchart explaining the method applied in this study; intensity–duration–frequency (IDF), adaptive mesh refinement (AMR).

## 2.2. Data and Methodology

### 2.2.1. Climate Change Scenarios

In general, SSPs consider multiple feasible trends in the social and natural systems that may develop over the 21st century. They comprise two elements: a set of quantized measurements of development and a narrative storyline [12]. Table 1 summarizes the SSP narratives considered in this study. The impact assessment of climate change carried out in this study mainly focused on a statistical trend analysis, based on the observations and the variables of the GCM output. GCMs generally have a large uncertainty, resulting in various resolutions and dynamic systems among the considered scenarios. Therefore, it is necessary to select appropriate scenarios or utilize all the available scenarios [13,14]. In general, the precipitation simulated by raw GCMs contains systematic errors. This is known as “bias”, which indicates a difference between observation and simulation [15,16]. Therefore, it is necessary to post-process the climate model output to replicate the observed climate through bias correction. Quantile mapping (QM) is a bias correction method and can be downscaled to the scale of the observation station. In this study, we used QM to produce a downscaled regional climate scenario.

**Table 1.** Details of the global circulation models (GCMs) used in this study.

Institute	GCM(s)	Resolution	Reference
Geophysical Fluid Dynamics Laboratory (USA)	GFDL-ESM4	360 × 180	[17]
Meteorological Research Institute (Japan)	MRI-ESM2-0	320 × 160	[18]
Centre National de Recherches Météorologiques (France)	CNRM-CM6-1	24,572 grids distributed over 128 latitude circles	[19]
	CNRM-ESM2-1		[20]
Institute Pierre-Simon Laplace (France)	IPSL-CM6A-LR	144 × 143	[21]
Max Planck Institute for Meteorology (Germany)	MPI-ESM1-2-HR	384 × 192	[22]
Met Office Hadley Centre (UK)	UKESM1-0-LL	192 × 144	[23]

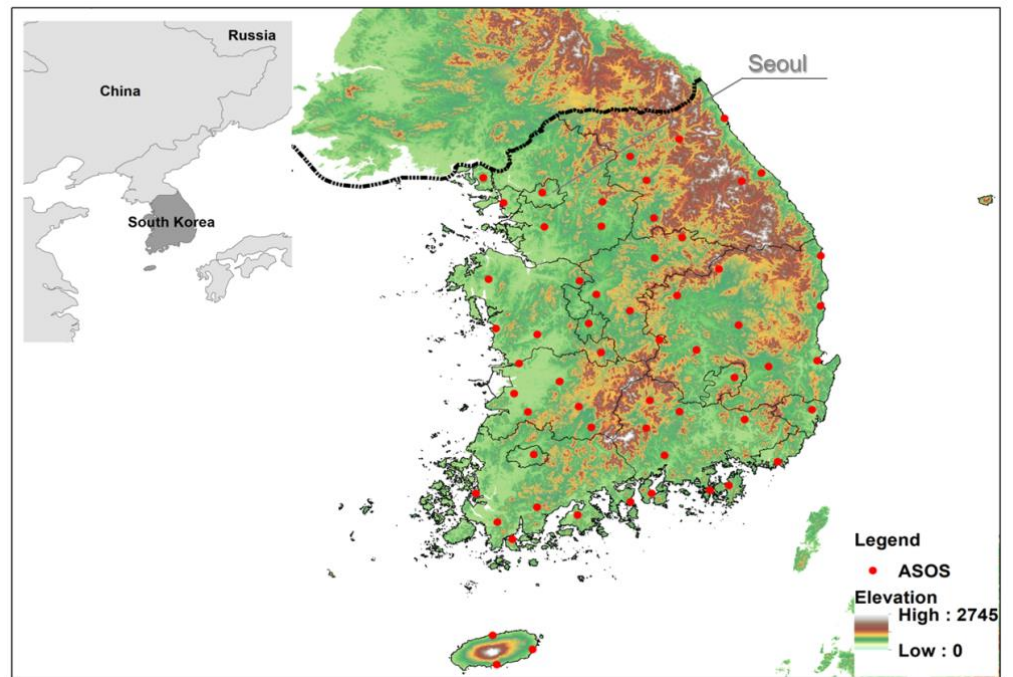
Table 1. Cont.

Institute	GCM(s)	Resolution	Reference
Commonwealth Scientific and Industrial Research Organisation, Australian Research Council Centre of Excellence for Climate System Science (Australia)	ACCESS-CM2	192 × 144	[24]
Commonwealth Scientific and Industrial Research Organisation (Australia)	ACCESS-ESM1-5	192 × 145	[25]
Canadian Centre for Climate Modelling and Analysis (Canada)	CanESM5	128 × 64	[26]
Institute for Numerical Mathematics (Russia)	INM-CM4-8	180 × 120	[27]
	INM-CM5-0	180 × 120	[28]
EC-Earth-Consortium	EC-Earth3	512 × 256	[29]
Japan Agency for Marine–Earth Science and Technology/Atmosphere and Ocean Research Institute/National Institute for Environmental Studies/RIKEN Center for Computational Science (Japan)	MIROC6	256 × 128	[30]
	MIROC-ES2L	128 × 64	[31]
NorESM Climate Modeling Consortium consisting of CICERO (Norway)	NorESM2-LM	144 × 96	[32]
National Institute of Meteorological Sciences/Korea Meteorological Administration (Republic of Korea)	KACE-1-0-G	192 × 144	[33]

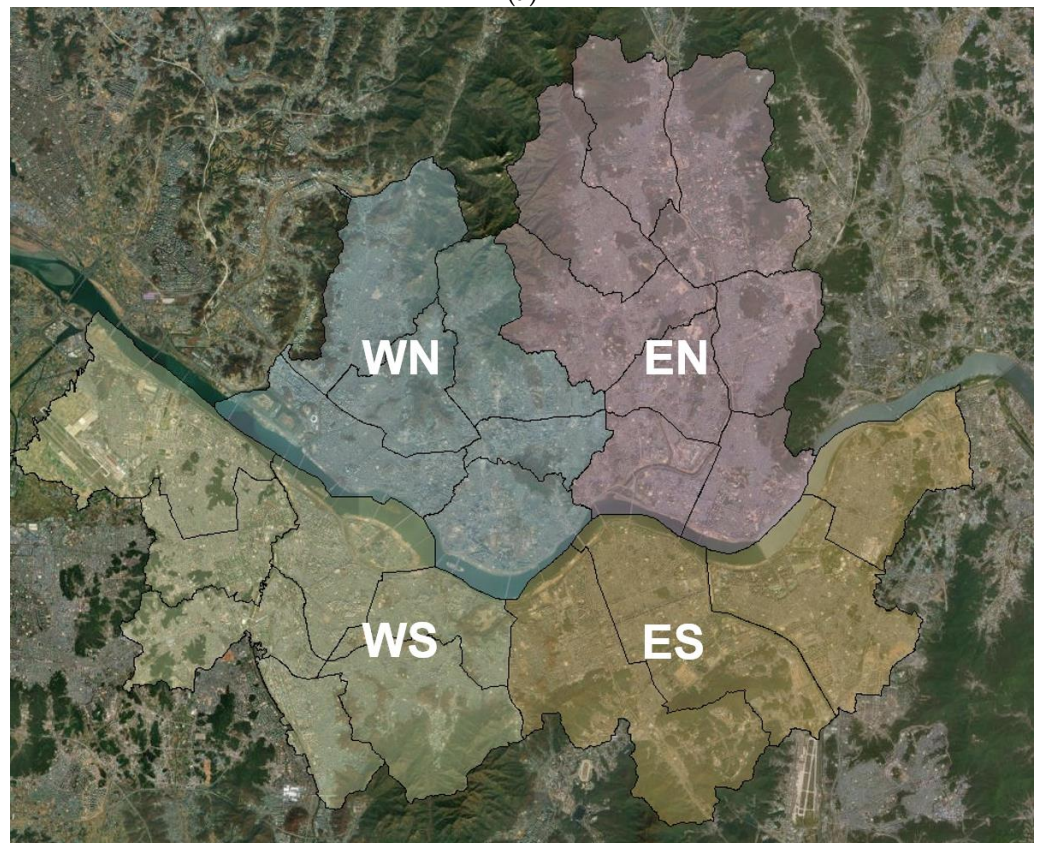
Notably, in this study, the temporal resolution of the GCM data was 1 day, and the spatial resolution was the station scale; among the four scenarios, SSP245, with an additional radiative forcing of  $4.5 \text{ W/m}^2$  by the year 2100, represents the medium pathway of future greenhouse gas emissions. In this scenario, we assumed that climate protection measures were implemented. A total of 17 GCMs were used for SSP245 (Table 1). The daily rainfall data of these GCMs were provided to 61 automated synoptic observing system (ASOS) stations by applying QM (Figure 2a). The Korea Meteorological Administration has assigned distinctive names to four regions within Seoul, representing the Northwest (WN), Southwest (WS), Northeast (EN), and Southeast (ES) regions, as illustrated in Figure 2b.

#### 2.2.2. Calculation of Intensity–Duration–Frequency (IDF) Using the Scaling-Generalized Extreme Value (GEV) Distribution Model

As shown in the figure, the daily and sub-daily extreme values were fitted to the scaling-GEV distribution model, and a scale between the daily GEV statistics and sub-daily extreme values was applied to future climate change scenarios for each duration. Furthermore, we tried to determine the probability of rainfall for the study area. We assumed that the statistical scale of the daily and sub-daily extreme values was constant while focusing on the fact that the first, second, and third moments decreased with a constant exponent when downscaled from the daily to the sub-daily values. The relationships among the shape, scale, and location parameters [Equations (2)–(4)] in the GEV distribution [Equation (1)] obtained for maximum rainfall at each duration were identified; the relationships determined from the observations were applied to the future climate change scenarios.



(a)



(b)

**Figure 2.** Maps of the (a) location of the automated synoptic observing system (ASOS) stations in South Korea and (b) the study area (Seoul); Northwest (WN), Southwest (WS), Northeast (EN), and Southeast (ES).

$$F(x) = \exp \left[ - \left( 1 - \kappa \frac{(x - \xi)}{\alpha} \right)^{\frac{1}{\kappa}} \right] \quad (1)$$

$$\kappa(\lambda t) = \kappa(t) \quad (2)$$

$$\alpha(\lambda t) = \lambda^\beta \alpha(t) \quad (3)$$

$$\xi(\lambda t) = \lambda^\beta \xi(t) \quad (4)$$

$$X_T(\lambda t) = \lambda^\beta X_T(t) \quad (5)$$

As we used the 1 day data for the future climate change scenarios to downscale the data into 24 h rainfall data, we constructed a time series of 24 h maximum and daily maximum rainfall from the observations; the correlation between the 1 day and 24 h annual maximum values was obtained, using Equation (6):

$$h_{24h} = \alpha_1 + \alpha_2 h_{1d} \quad (6)$$

### 3. Result

#### 3.1. Characteristics of Heavy Rainfall That Occurred in Seoul in 2022

Figure 3 shows the rainfall data for 8–10 August 2022. The rainfall was mainly concentrated in the 37°–38° N latitude, and there were large spatial variations in the study area, even within the Seoul area (Figure 3). As shown in Figure 2, we divided Seoul into four regions, namely Northwest (WN), Southwest (WS), Northeast (EN), and Southeast (ES); we used the rainfall data acquired from 27 meteorological observations in the Seoul area for the study period.

The maximum rainfall for each duration was obtained by determining the hourly moving average rainfall and summing the above 3-day rainfall time series. In the figure, the bars represent the maximum rainfall for 1, 3, 6, 9, 12, 18, 24, 36, and 72 h by region, and the black line denotes the annual maximum rainfall for each duration obtained from Seoul from 1961 to 2017; the plain, dotted, and dashed black lines represent the maximum, average, and minimum values. There was a large difference in the maximum rainfall by the duration between the different regions of the study area, and the maximum rainfall in the ES (red) and WS (gray) regions was greater than that in the EN and WN. In particular, the maximum rainfall for a duration of 12 h or less was similar to or greater than the historical maximum of Seoul (Figure 4).

The cumulative distribution function was estimated by fitting the GEV distribution to the annual maximum rainfall for each duration, and the return periods of these rainfall events were inverted from the cumulative distribution function. The WS region had a duration of more than 30 years (from 3 to 12 h); in particular, the precipitation of the 3 h and 12 h duration had a return period of more than 50 years. In the ES region, the frequency was approximately 20 years, and the return period of the 12 h precipitation duration was approximately 24 years, but in the EN and WN regions, it was approximately 5 years for the entire duration (Figure 5).

The impact of climate change was assessed in various fields, using the Special Report on Emission Scenarios (SRES) and the RCP and SSP scenarios. In particular, the quantification of uncertainty and the application of downscaling techniques are key issues in projecting extreme rainfall, with several studies being conducted in South Korea as well. Since the 5th Assessment Report, in which the daily projection system was established, the change in the annual maximum daily rainfall in the future, relative to the projection climate, was projected; this method can provide the most common and intuitive results.

For example, the authors of [34] downscaled the long-term trends for extreme values to 26 RCP scenarios to examine the impact of climate change.

Figure 6 represents the 20-year frequency daily rainfall projected for the present and future periods, indicating an increasing trend in the future, relative to the current trend. The increase was evident in the 37°–38° N latitude region and the southern coastal area. Figure 6b represents F1 (indicating the future scenario for 2011–2040), and the climate we are experiencing corresponds to this. In most of the 26 climate change scenarios, extreme rainfall in the region around 37°–38° N was projected to increase, illustrating a similar trend to that of the current cumulative rainfall (Figure 3d).

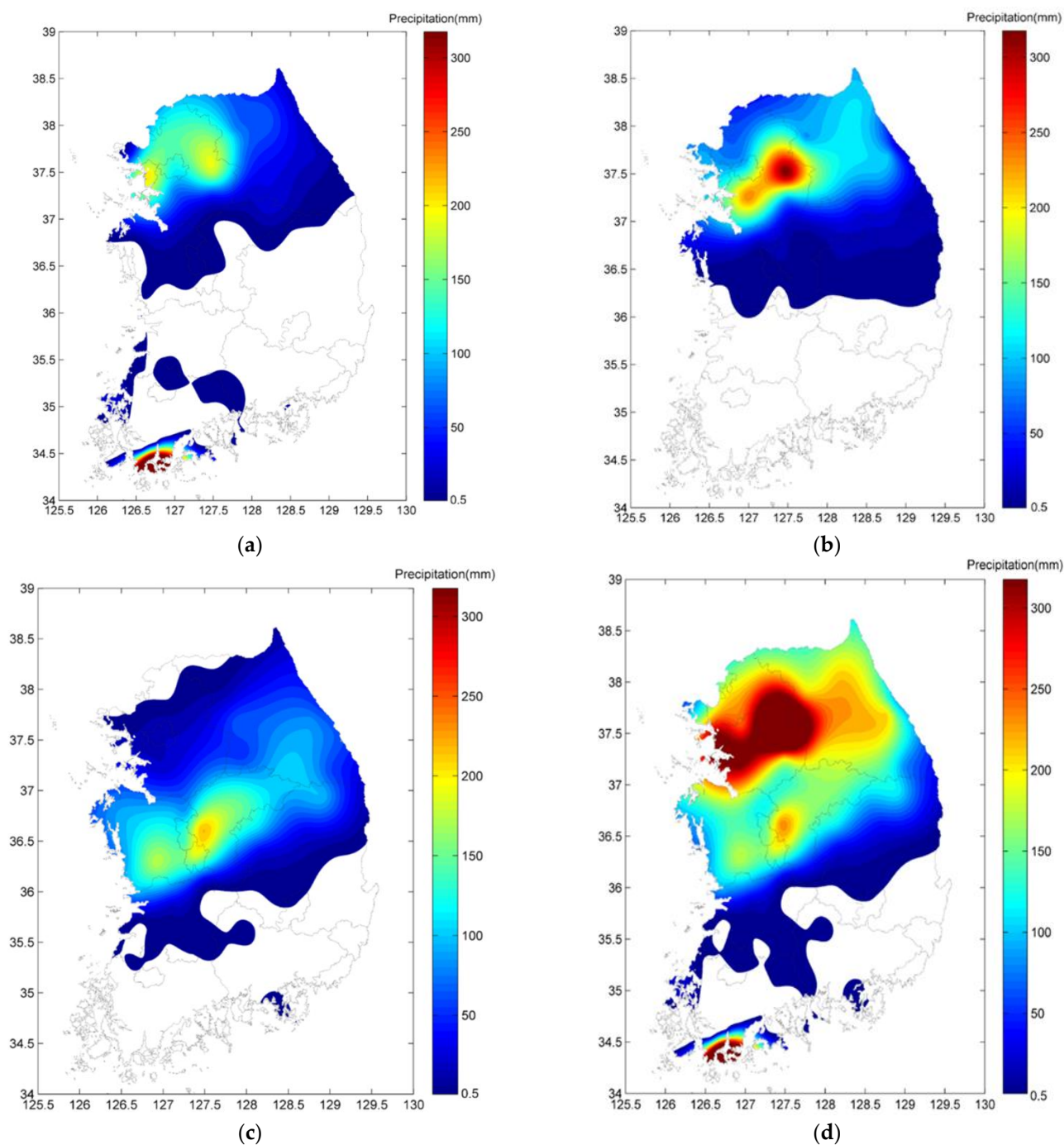


**Figure 3.** Rainfall during 8–10 August 2022. (a) Rainfall on 8 August 2022; (b) Rainfall on 9 August 2022; (c) Rainfall on 10 August 2022; (d) Cumulative rainfall during 8–10 August 2022.

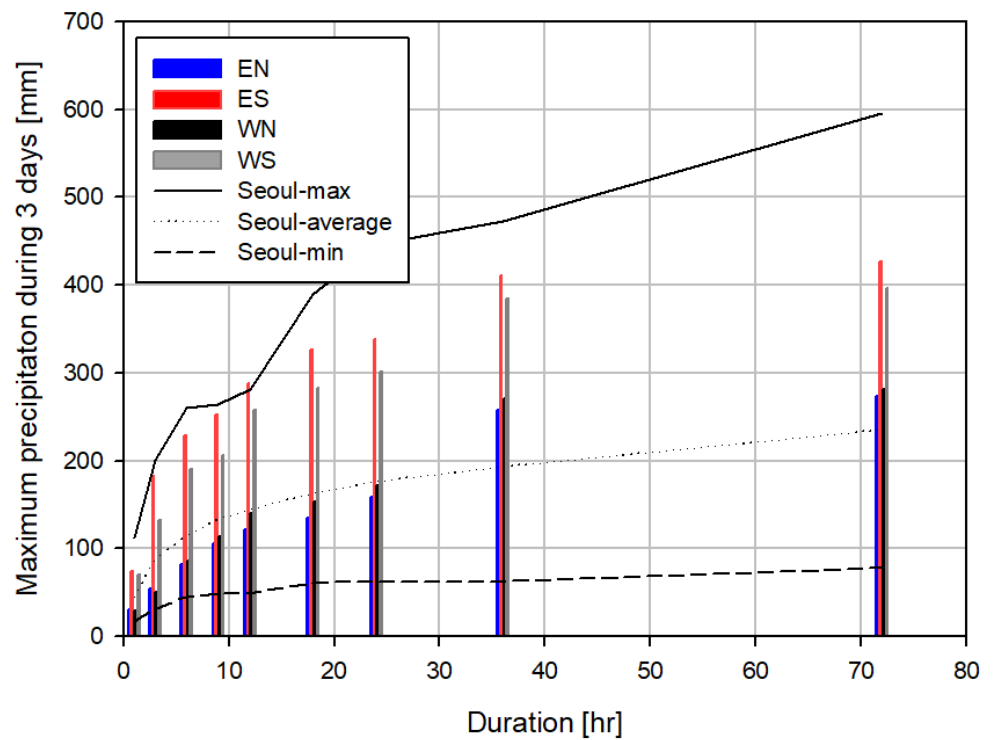


Figure 4. The plot of maximum recorded rainfall during 8–10 August 2022 vs. duration.

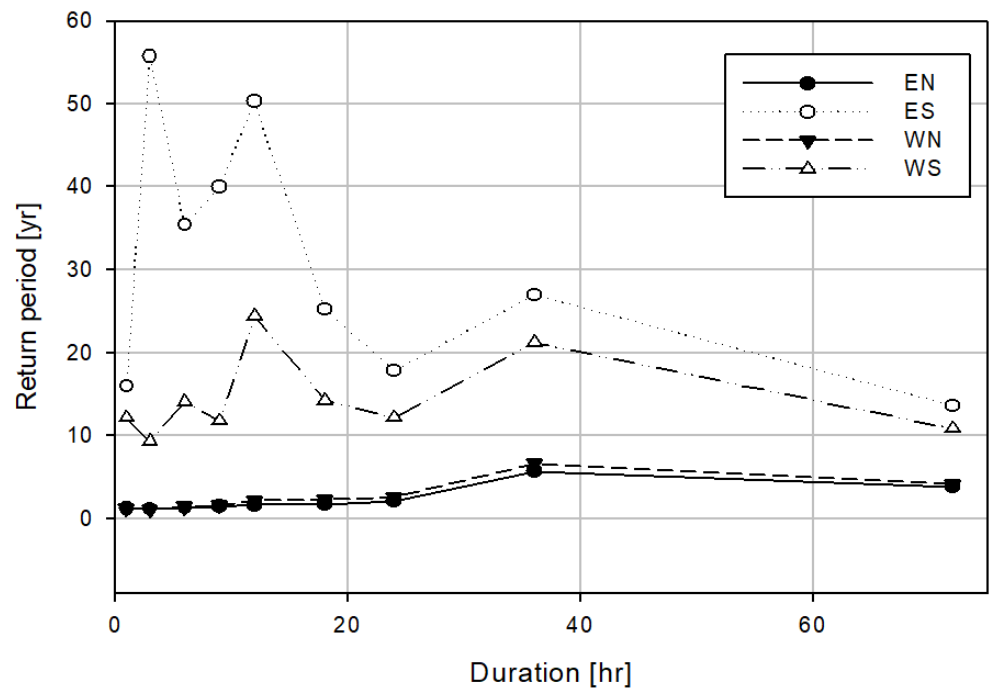
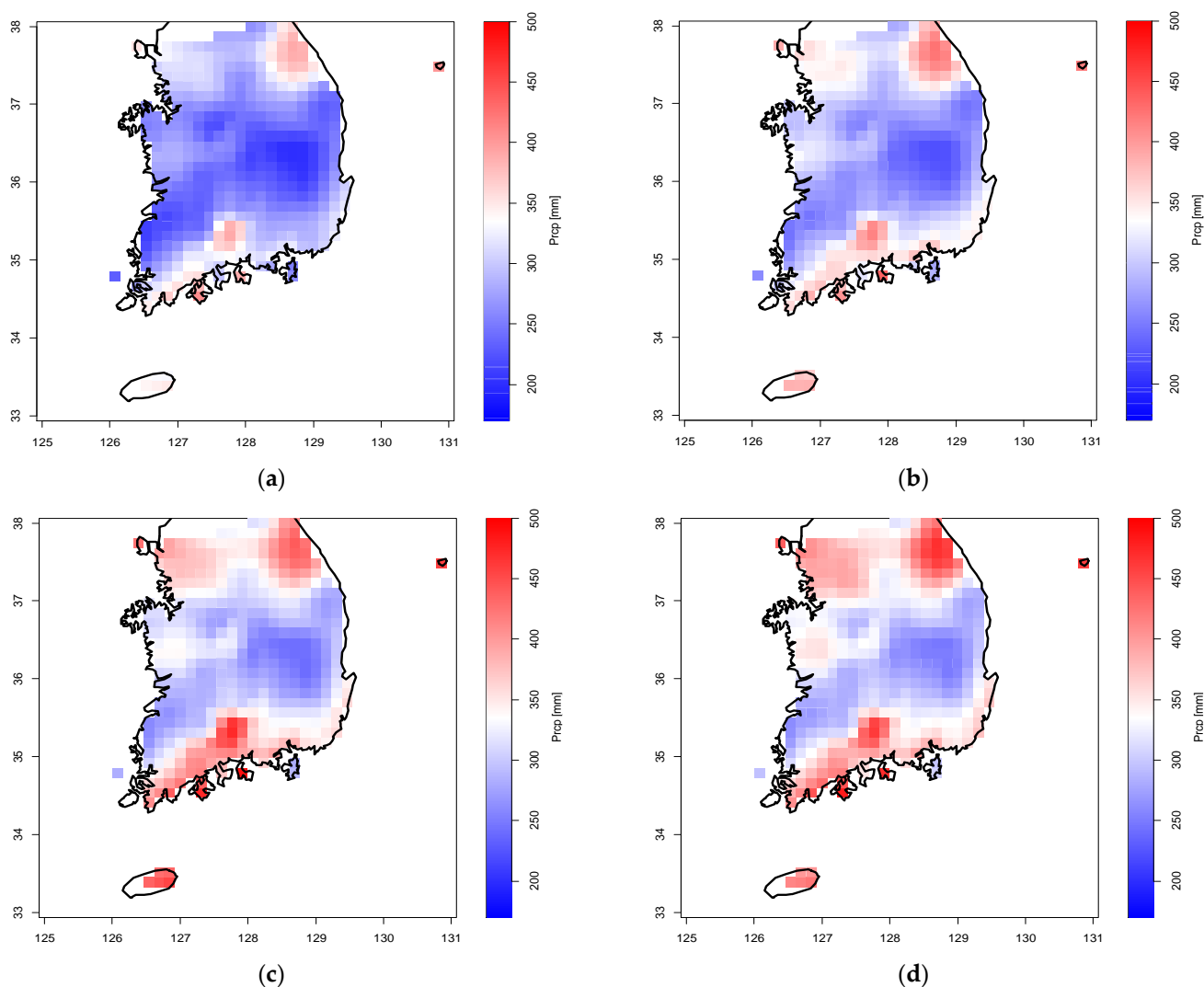


Figure 5. Return periods of annual maximum rainfall events by duration.

In terms of the frequency changes, Figure 7 shows a projection of future changes in the 20-year frequency in the present climate, indicating that the annual maximum daily rainfall corresponding to the present 20-year frequency may occur more frequently in the future. Specifically, it would decrease to 16.6 years in F1, 14.1 years in F2, and finally, 12.8 years in F3. Compared to Figure 5, the 24 h precipitation levels in the ES and WS regions would decrease to 17.8 and 12.2 years, respectively.



**Figure 6.** Twenty-year frequency rainfall for the present (1980–2005) and the future scenarios for 2011–2040 (Future 1, F1), 2041–2070 (Future 2, F2), and 2071–2100 (Future 3, F3) [34]. (a) Present: 1980–2005; (b) F1: 2011–2040; (c) F2: 2041–2070; (d) F3: 2071–2100.

### 3.2. Projection of Future Intensity–Duration–Frequency (IDF) for SSP245

Before constructing the IDF curves for each duration, we investigated the performance of 17 climate change scenarios, according to the SSP245 and downscaled to a station scale. Notably, we calculated the spatial distribution and coefficient of variance (CV) of the ensemble mean of the 20-year frequency maximum daily rainfall. Figure 8 presents the 20-year frequency rainfall obtained by fitting the GEV distribution with the maximum likelihood method (F1: 2011–2040, F2: 2041–2070, and F3: 2071–2100). The ensemble average of the 20-year frequency rainfall in the present climate scenario across South Korea is 246.8 mm, and it is projected that the rainfall will increase in the future.

Figure 9 shows the CV (coefficient of variation) of the maximum daily rainfall of the 20-year frequency among the 17 GCM models at each observation site considered in this study; it was calculated by dividing the average of the GCMs at each site by the standard deviation. Specifically, we converted daily data into 24 h data using temporal downscaling (linear regression) and converted it into 1 h data by using a scaling method on the 24 h data. Therefore, we analyzed the inter-model variability for daily data. As a result, the CV increased with time, indicating that the variability (uncertainty) of and among the models will increase in the far future. The CV for the ensemble mean of the 20-year frequency

rainfall in the present climate scenario was 0.064 (as the spatial average), and the value can be expected to increase in the future (to 0.212 in F1, 0.215 in F2, and 0.220 in F3).

Based on the linear relationship between the observed 1-day and 24 h maximum time series, the 17 annual maximum daily rainfall time series in the future were converted into 24 h duration time series, and the 20-year frequency rainfalls in the present and future climate scenarios were estimated by fitting them to the GEV distribution model. Compared to the daily maximum rainfall, the 24 h frequency rainfall was greater, but the latter's spatial distribution was similar to the daily maximum rainfall; as a result of the comparison of the ensemble averages, an increase can be expected in the future, compared to that in the present climate scenario (266.6 mm). Notably, the rainfall during F1, F2, and F3 was estimated to be 288.6, 302.8, and 315.5 mm, respectively (Figure 10).

The GEV parameters of the 24 h maximum precipitation over the whole of South Korea were averaged, and the location and scale parameters of the present and F3 scenarios were 149.3 and 47.4, respectively, which were larger than those of the present (130.7 and 39.4). Furthermore, the shape parameter decreased from 0.153 to 0.095 in the present climate scenario, and based on this, we projected the changes in the present and future climate change scenarios of PDF (probability density function). As the location and scale parameters increased, the PDF moved to the right, its width widened, and the right tail became thicker, due to the decrease in the shape parameter. Thus, a thicker right tail indicates that the occurrence frequency of extreme rainfall events will increase in the future (Figure 11a). Due to these PDF changes, the 20-year return period will decrease in the future, compared to that in the present climate scenario, and can be expected to decrease to 14.3 years in the F3 (2071–2100) scenario (Figure 11b).

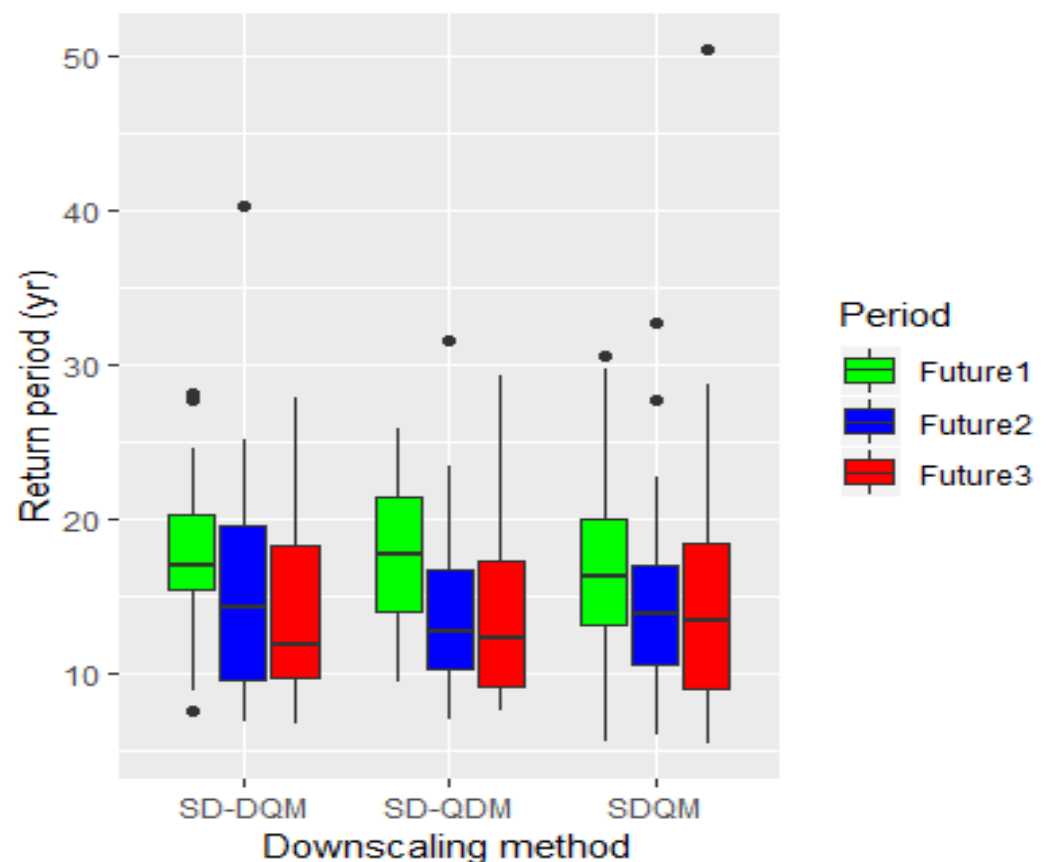
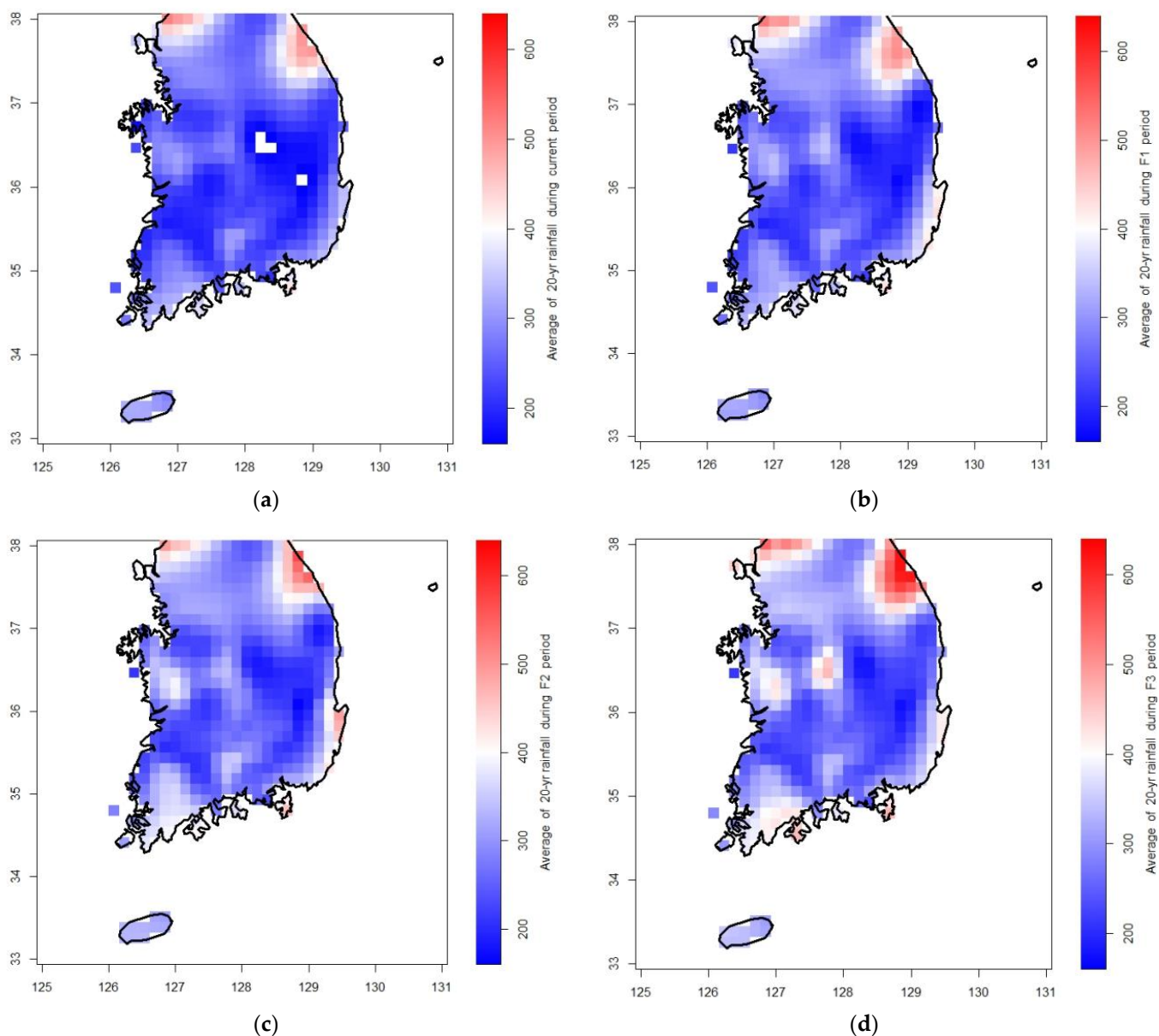
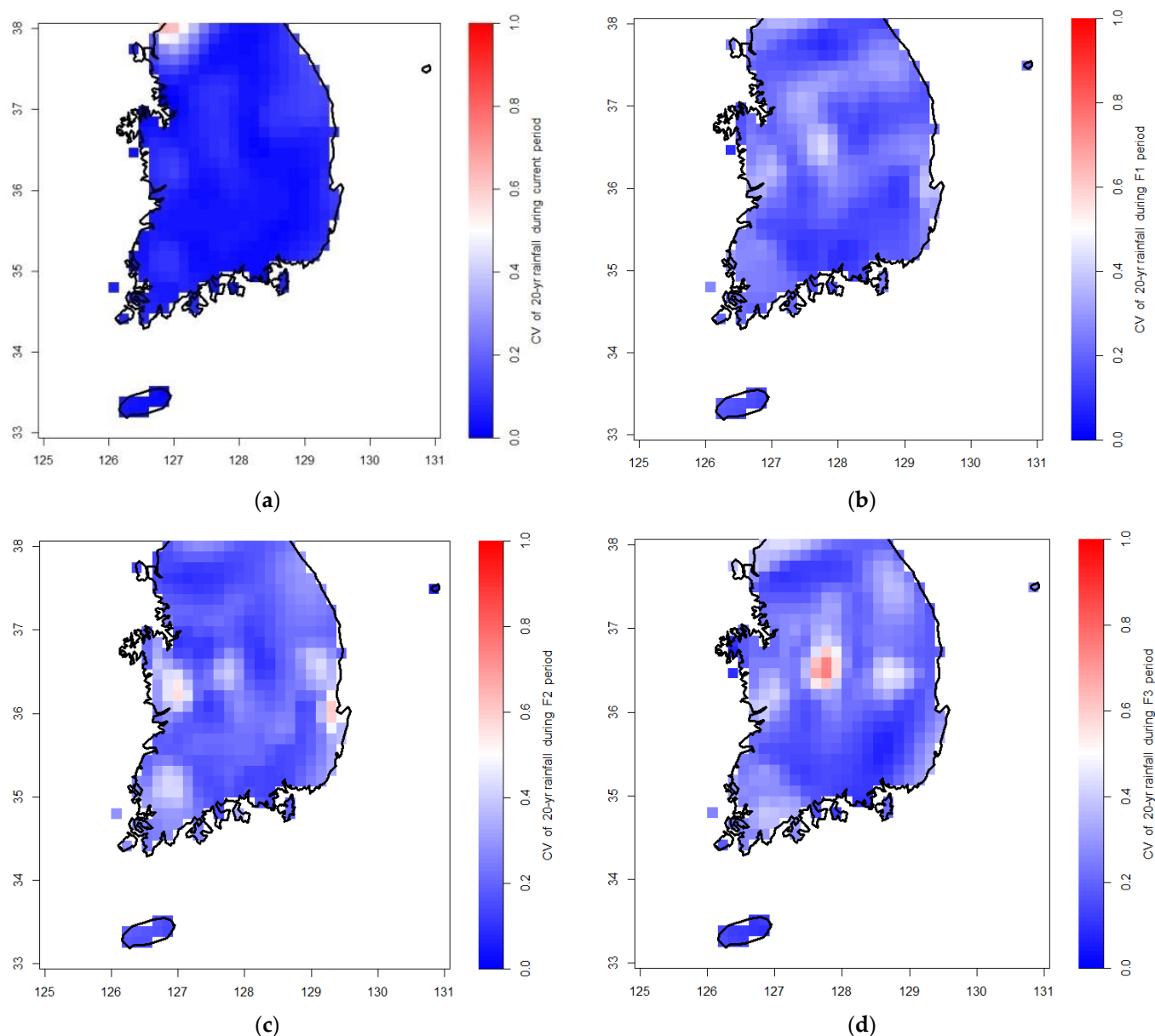


Figure 7. The projection of future changes of the present 20-year return period [34].



**Figure 8.** Ensemble averages of 20-year frequency daily maximum rainfall in the present and future climate scenarios, based on the 17 global climate models (GCMs) considered in this study. (a) Present: 1980–2005; (b) F1: 2011–2040; (c) F2: 2041–2070; (d) F3: 2071–2100.

In 2022, Seoul experienced urban flooding, resulting from multiple extreme rainfall events over a short duration. In this study, the resolution of the 24 h duration was detailed using a scale index, with a resolution of 1 h. The scaling exponent was estimated using the moment for each duration, based on a single scale. First, the 1st to 5th order moments were calculated for each duration of the rainfall data, and the first moment up to the 5th order moment was plotted for each duration on the logarithmic scale, to calculate the scale index (Figure 12a). Figure 12b represents the slope of the linear regression for each order estimated using these values, and the slope of the moment  $\ln$  for the moment order  $l$  was considered as the scaling exponent for each moment order (Figure 12b).



**Figure 9.** Inter-model variability of the 20-year frequency maximum daily rainfall uncertainty in the present and future climate scenarios, based on the 17 global climate models (GCMs) considered in this study. (a) Present: 1980–2005; (b) F1: 2011–2040; (c) F2: 2041–2070; (d) F3: 2071–2100.

The IDF was projected by applying a power of (0.462) to the ratio of individual durations (1, 3, 6, 12, and 18) in relation to a 24, subsequently multiplied by the 24 h rainfall amount. (Figure 13). The graph of the rainfall intensity for the durations of 1, 3, and 6 h is shown in Figure 13a, and the graph of the rainfall intensity for the durations of 12, 18, and 24 h is shown in Figure 13b. Figure 13a, in which we consider a relatively short duration, is related to urban flooding, and Figure 13b is related to river flooding. In particular, the maximum rainfall per hour portrayed in Figure 13a is a major variable for the design of the urban drainage system, and is projected to be 100.0 mm/h (F3 period). In addition, extreme rainfall over a long duration (Figure 13b) was the strongest in the F1 scenario; therefore, we suggest the urgent development and implementation of relevant measures to prevent and mitigate not only urban flooding but also river flooding.

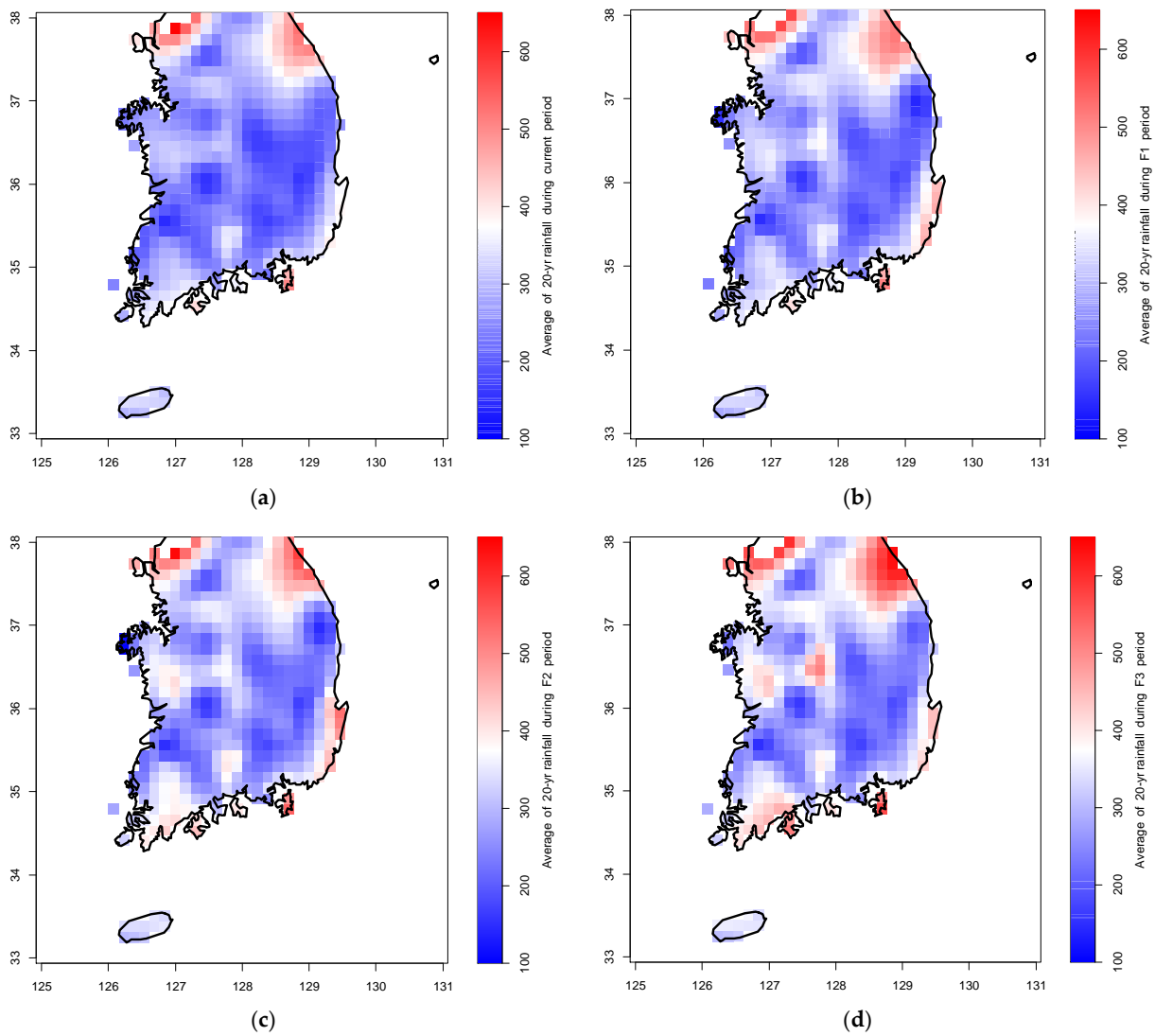


**Figure 10.** Change in 20-year frequency rainfall during (a) present (1980–2005) and (b–d) future scenarios (F1: 2011–2040; F2: 2041–2070; and F3: 2071–2100, respectively). (a) Present: 1980–2005; (b) F1: 2011–2040; (c) F2: 2041–2070; (d) F3: 2071–2100.

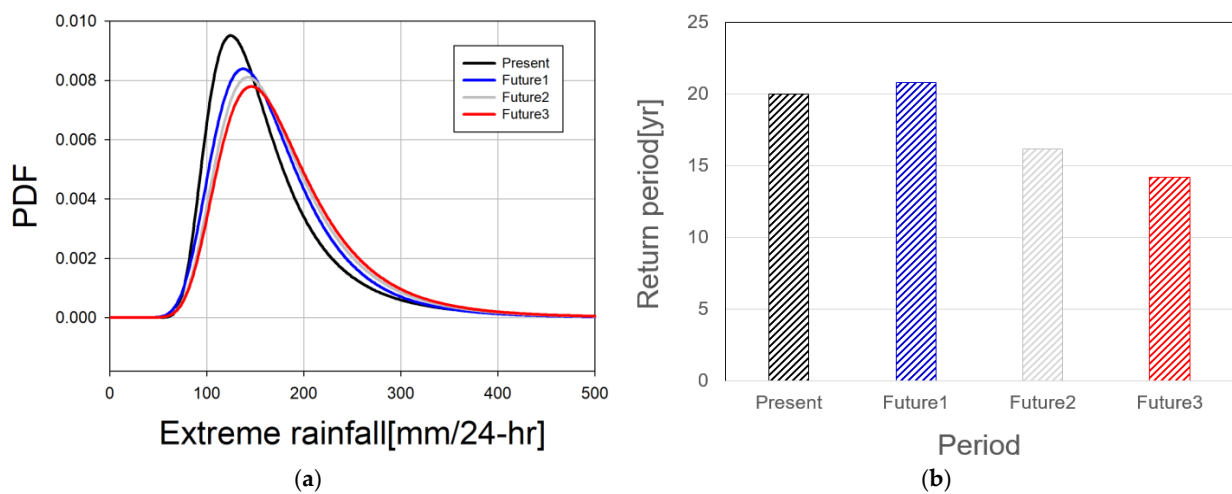


**Figure 11.** Changes in the (a) probability density function (PDF) and (b) return period. (a) Shift in the PDF; (b) changes in return period.

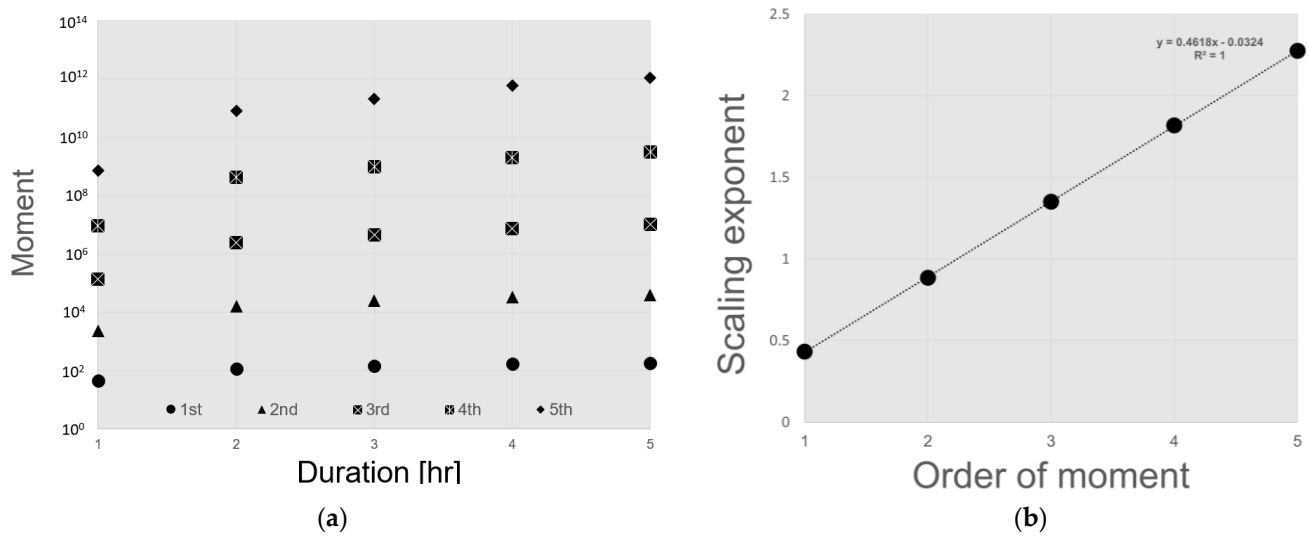


**Figure 12.** The slope of the linear regression for each order. (a) Scaling of moments with duration; (b) simple scaling.

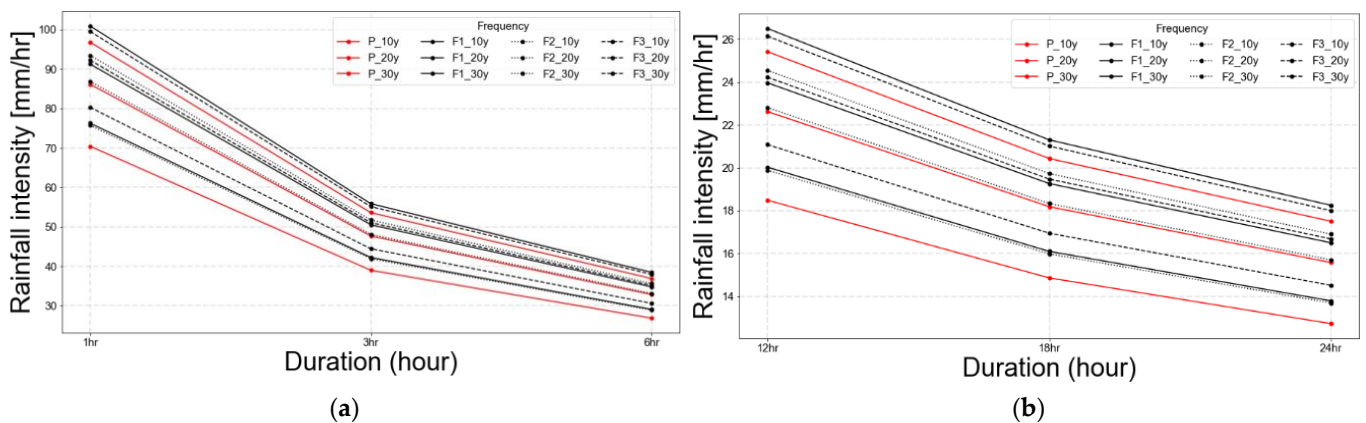


**Figure 13.** Projected intensity–duration–frequency (IDF) curves for Seoul. (a) Rainfall intensity for the durations of 1, 3, and 6 h; (b) Rainfall intensity for the durations of 12, 18, and 24 h.

#### 4. Conclusions

In this study, we analyzed the characteristics of extreme rainfall events that occurred in South Korea in 2022 and projected the future change in the maximum rainfall, at temporal resolutions of 1 day/24 h, based on 17 SSP245 scenarios. The frequency of the maximum 24 h rainfall data recorded in the ES and WS regions of Seoul in 2022 was estimated to be 17.8 and 12.2 years, respectively, very similar to the return period in F1 projected in the RCP climate change scenario. The results of this study confirm that the climate change presented in previous studies is now a reality, indicating that we are currently experiencing a climate crisis. As the heavy rainfall event in Seoul occurred over a short period and had a strong intensity, the city experienced large-scale urban flooding.

Therefore, the IDF curves, which reflect climate change at the sub-daily scale, can be used to improve the infrastructure design of the city to prepare for future urban flooding events. Therefore, in this study, the exceedance probability of maximum rainfall in the future was projected based on different SSP scenarios; the results indicate an increase in the maximum rainfall in the future. The 24 h maximum rainfall projected for the future, obtained by applying the relationship of the 1-day/24 h annual maximum series (based on actual observations) to the climate change scenarios, will increase by about 18% (relative to the current conditions); the 20-year frequency will be 14.3 years, and the return period will shorten.

The future IDF curve for Seoul was projected by applying the scaling-GEV method for the 24 h duration maximum precipitation series; we assumed that the scaling index was the same as the historical observation. The duration considered in this study ranged from 24 h to 1 h; the strongest rainfall intensity can be expected in F1, regardless of the duration. In particular, as Seoul has a very high urbanization rate, the probability of flooding was very high, owing to the heavy rain and short duration. Based on the RCP climate change scenario, we determined that at present, we are in the midst of a climate change crisis; furthermore, we could estimate that the crisis will escalate in F1, based on the SSP scenario.

Notably, as we are in the midst of a climate change crisis, measures to manage the floods in cities and rivers must be established. In other words, in F1, there will be a very high possibility of floods at a scale that we have never experienced before; therefore, we urgently need to prepare for such events. To respond to changing extreme events, upward adjustments in the design level are inevitable. However, such upward adjustments cannot resolve all the problems associated with urban planning and natural hazards. In addition, considering the stochastic characteristics of the hydrologic time series, we will experience more extreme rainfall events in the future. The occurrence of extreme rainfall exceeding the design level can lead to increased damage in the future.

Therefore, it is necessary to implement non-structural methods, such as forecasting, to address such issues. The selection of appropriate investigation equipment (through the development of investigation technology) and the accumulation of high-quality data (through data quality control) are crucial for urban flood forecasting. In addition, using sensor data, which is the main technology of the 4th industrial revolution, data linkage (using the Internet of Things), artificial intelligence-based automatic quality control, and data verification (using intelligent CCTV) can be useful for urban flood forecasting.

## 5. Discussion

As the climate change scenarios considered in this study were developed using different dynamics, the uncertainties of these models are large. In spite of the large uncertainty among the different models, e.g., the strong signal (spatial distribution, etc.), can mean that it can occur more reliably. Based on a study conducted by ref. [34], the CVs of the GCMs of the 20-year frequency daily maximum rainfall (detailed by the QM), according to the RCP, were 0.132 (present), 0.235 (F1), 0.235 (F2), and 0.234 (F3). Based on the uncertainty range estimated in previous studies, the extreme rainfall in this summer could be explained as a climate change scenario. According to our study, the CV, which was 0.064 in the present climate scenario, is expected to increase in the future: 0.212 in F1, 0.215 in F2, and 0.220 in F3. In other words, the variability between the models was lower than that of the RCPs; based on these data, we estimate with great certainty that there will be an increase in extreme rainfall events in the future.

Many studies have employed a combination of multiple climate models to assess the degree of the climate crisis ([35–37]). Despite the increasing evidence, skepticism persists regarding the severity of projected global warming, with some arguing for potential overestimation. However, [38] presented a comprehensive analysis, comparing observations with future temperature projections from the CMIP3, CMIP5, and CMIP6 models. Their findings caution that the future warming projections provided by CMIP may have been somewhat underestimated. This implies that the current climate crisis may transition from a transient phase to a more enduring regime. Consequently, a heightened incidence of atmospheric rivers is anticipated, due to the sustained influx of water vapor. We did not quantify the precise relationship between atmospheric rivers and climate change. Therefore, we intend to explore alterations in patterns of intense rainfall, induced by escalating temperatures within the future climate system.

**Author Contributions:** Conceptualization, J.H.S. and B.S.K.; analysis and writing, J.H.S. and Y.-H.S.; Data collection and figure creation, J.H.S. and D.H.K. All authors have read and agreed to the published version of the manuscript.

**Funding:** This research was supported by a grant (RS-2023-00244860) of the Policy-linked Technology Development Program on Natural Disaster Prevention and Mitigation funded by the Ministry of Interior and Safety (MOIS, Republic of Korea).

**Data Availability Statement:** Data are contained within the article.

**Conflicts of Interest:** The authors declare no conflict of interest.

## References

1. Min, S.-K.; Zhang, X.; Zwiers, F.W.; Hegerl, G.C. Human contribution to more-intense precipitation extremes. *Nature* **2011**, *470*, 378–381. [[CrossRef](#)]
2. Westra, S.; Fowler, H.J.; Evans, J.P.; Alexander, L.V.; Berg, P.; Johnson, F.; Kendon, E.J.; Lenderink, G.; Roberts, N.M. Future changes to the intensity and frequency of short-duration extreme rainfall. *Rev Geophys.* **2014**, *52*, 522–555. [[CrossRef](#)]
3. Milly, P.C.D.; Betancourt, J.; Falkenmark, M.; Hirsch, R.M.; Kundzewicz, Z.W.; Lettenmaier, D.P.; Stouffer, R.J. Stationarity is dead: Whither water management? *Science* **2008**, *319*, 573–574. [[CrossRef](#)]
4. Kendon, E.J.; Stratton, R.A.; Tucker, S.; Marsham, J.H.; Bethou, S.; Rowell, D.P.; Sejior, C.A. Enhanced future changes in wet and dry extremes over Africa at convection-permitting scale. *Nat. Commun.* **2019**, *10*, 1794. [[CrossRef](#)]
5. Martel, J.L.; Brissette, F.P.; Lucas-Picher, P.; Troin, M.; Arsenaault, R. Climate Change and Rainfall Intensity-Duration-Frequency Curves: Overview of Science and Guidelines for Adaptation. *J. Hydrol. Eng.* **2021**, *26*, 03121001. [[CrossRef](#)]
6. Buonomo, E.; Jones, E.; Huntingford, C.; Hammafard, J. On the robustness of changes in extreme precipitation over Europe from two high resolution climate change simulations. *Q. J. R. Meteorol. Soc.* **2007**, *133*, 65–81. [[CrossRef](#)]
7. Kwon, M.; Sung, J.-H.; Ahn, J. Change in extreme precipitation over North Korea using multiple climate change scenarios. *Water* **2019**, *11*, 270. [[CrossRef](#)]
8. Nguyen, V.; Desramaut, N.; Nguyen, T. Estimation of urban design storms in consideration of GCM-based climate change scenarios. In Proceedings of the International Conference on Water & Urban Development Paradigms: Towards an Integration of Engineering, Design and Management Approaches, Leuven, Belgium, 15–17 September 2008; pp. 347–356.
9. Vu, M.; Raghavan, S.; Liu, J.; Liong, S.Y. Constructing short-duration IDF curves using coupled dynamical–statistical approach to assess climate change impacts. *Int. J. Climatol.* **2018**, *38*, 2662–2671. [[CrossRef](#)]
10. Choi, J.; Lee, O.; Jang, J.; Jang, S.; Kim, S. Future intensity–depth–frequency curves estimation in Korea under representative concentration pathway scenarios of fifth assessment report using scale-invariance method. *Int. J. Climatol.* **2019**, *39*, 887–900. [[CrossRef](#)]
11. Yeo, M.-H.; Nguyen VT, V.; Kpodonu, T.A. Characterizing extreme rainfalls and constructing confidence intervals for IDF curves using Scaling-GEV distribution model. *Int. J. Climatol.* **2021**, *41*, 456–468. [[CrossRef](#)]
12. O’Neill, B.C.; Krigler, E.; Rhiahi, K.; Ebi, K.L.; Hallegatte, S.; Carter, T.R.; Mathur, R.; van Vuuren, D.P. A new scenario framework for climate change research: The concept of shared socioeconomic pathways. *Clim. Chang.* **2014**, *122*, 387–400. [[CrossRef](#)]
13. Song, Y.-H.; Chung, E.-S.; Shiru, M.S. Uncertainty analysis of monthly precipitation in GCMs using multiple bias correction methods under different RCPs. *Sustainability* **2020**, *12*, 7508. [[CrossRef](#)]
14. Homsy, R.; Shiru, M.S.; Shahid, S.; Ismail, T.; Harun, S.B.; Al-Ansari, N.; Chau, K.W.; Yaseen, Z.M. Precipitation projection using a CMIP5 GCM ensemble model: A regional investigation of Syria. *Eng. Appl. Comput. Fluid Mech.* **2020**, *14*, 90–106. [[CrossRef](#)]
15. Pierce, D.W.; Cayan, D.R.; Maurer, E.P.; Abatzoglou, J.T.; Hegewisch, K.C. Improved bias correction techniques for hydrological simulations of climate change. *J. Hydromet.* **2015**, *16*, 2421–2442. [[CrossRef](#)]
16. Maraun, D. Bias correction, quantile mapping, and downscaling: Revisiting the inflation issue. *J. Clim.* **2013**, *26*, 2137–2143. [[CrossRef](#)]
17. John, J.G.; Blanton, C.; McHugh, C.; Radhakrishnan, A.; Rand, K.; Vahlenkamp, H.; Wilson, C.; Zadeh, N.T.; Dunne, J.P.; Dussin, R. NOAA-GFDL GFDL-ESM4 Model Output Prepared for CMIP6 ScenarioMIP; Version 20180701; Earth System Grid Federation: Greenbelt, MD, USA, 2018.
18. Yukimoto, S.; Kawai, H.; Koshiro, T.; Oshima, N.; Yoshida, K.; Urakawa, S.; Tsujino, H.; Deushi, M.; Tanaka, T.; Hosaka, M. The meteorological research institute earth system model version 2.0, MRI-ESM2.0: Description and basic evaluation of the physical component. *J. Meteorol. Soc. Jpn. Ser. II* **2019**, *97*, 931–965. [[CrossRef](#)]
19. Voldoire, A.; Saint-Martin, D.; S n si, S.; Decharme, B.; Alias, A.; Chevallier, M.; Colin, J.; Gu r my, J.F.; Michou, M.; Moine, M.P. Evaluation of CMIP6 DECK Experiments With CNRM-CM6-1. *J. Adv. Model Earth Syst.* **2019**, *11*, 2177–2213. [[CrossRef](#)]
20. Seferian, R.; Nabat, P.; Michou, M.; Saint-Martin, D.; Voldoire, A.; Colin, J.; Decharme, B.; Delire, C.; Berthet, S.; Chevallier, M.; et al. Evaluation of CNRM Earth System Model, CNRM-ESM2-1: Role of Earth System Processes in Present-Day and Future Climate. *J. Adv. Model. Earth Syst.* **2019**, *11*, 4182–4227. [[CrossRef](#)]
21. Boucher, O.; Denvil, S.; Levavasseur, G.; Cozic, A.; Caubel, A.; Foujols, M.A.; Khodri, M.; Krinner, G.; Lebas, N.; Levavasseur, G.; et al. IPSL IPSL-CM6A-LR model output prepared for CMIP6 CMIP historical. Earth System Grid Federation. *J. Adv. Model. Earth Syst.* **2018**, *12*, e2019MS002010. [[CrossRef](#)]
22. Schupfner, M.; Wieners, K.H.; Wachsmann, F.; Steger, C.; Bittner, M.; Jungclaus, J.; Fr h, B.; Pankatz, K.; Giorgetta, M.; Reick, C. DKRZ MPI-ESM1. 2-HR Model Output Prepared for CMIP6 ScenarioMIP; Version 20190710; Earth System Grid Federation: Greenbelt, MD, USA, 2019.

23. Sellar, A.A.; Jones, C.G.; Mulcahy, J.P.; Tang, Y.; Yool, A.; Wiltshire, A.; O'Connor, F.M.; Stringer, M.; Hill, R.; Palmieri, J.; et al. UKESM1: Description and Evaluation of the U.K. Earth System Model. *J. Adv. Model. Earth Syst.* **2019**, *11*, 4513–4558. [[CrossRef](#)]
24. Dix, M.; Bi, D.; Dobrohotoff, P.; Fiedler, R.; Harman, I.; Law, R.; Mackallah, C.; Marsland, S.; O'Farrell, S.; Rashid, H. *CSIRO-ARCCSS ACCESS-CM2 Model Output Prepared for CMIP6 ScenarioMIP SSP585*; Version 20200303; Earth System Grid Federation: Greenbelt, MD, USA, 2019.
25. Ziehn, T.; Chamberlain, M.; Lenton, A.; Law, R.; Bodman, R.; Dix, M.; Wang, Y.; Dobrohotoff, P.; Srbinovsky, J.; Stevens, L. *CSIRO ACCESS-ESM1. 5 Model Output Prepared for CMIP6 ScenarioMIP SSP585*; Version 20191115; Earth System Grid Federation: Greenbelt, MD, USA, 2019.
26. Swart, N.C.; Cole, J.N.S.; Kharin, V.V.; Lazare, M.; Scinocca, J.F.; Gillett, N.P.; Anstey, J.; Arora, V.; Christian, J.R.; Jiao, Y. *CCCma CanESM5 Model Output Prepared for CMIP6 ScenarioMIP ssp585*; Version 20190429; Earth System Grid Federation: Greenbelt, MD, USA, 2019.
27. Volodin, E.; Mortikov, E.; Gritsun, A.; Lykossov, V.; Galin, V.; Diansky, N.; Gusev, A.; Kostykin, S.; Iakovlev, N.; Shestakova, A. *INM INM-CM4-8 Model Output Prepared for CMIP6 ScenarioMIP*; Version 20190603; Earth System Grid Federation: Greenbelt, MD, USA, 2019.
28. Volodin, E.; Mortikov, E.; Gritsun, A.; Lykossov, V.; Galin, V.; Diansky, N.; Gusev, A.; Kostykin, S.; Iakovlev, N.; Shestakova, A. *INM INM-CM5-0 Model Output Prepared for CMIP6 ScenarioMIP SSP585*; Version 20190724; Earth System Grid Federation: Greenbelt, MD, USA, 2019.
29. EC-Earth Consortium (EC-Earth). *EC-Earth-Consortium EC-Earth3 Model Output Prepared for CMIP6 CMIP Ab-rupt-4xCO2*; Version 20200501; Earth System Grid Federation: Greenbelt, MD, USA, 2019.
30. Shiogama, H.; Abe, M.; Tatebe, H. *MIROC MIROC6 Model Output Prepared for CMIP6 ScenarioMIP SSP585*; Version 20191114; Earth System Grid Federation: Greenbelt, MD, USA, 2019.
31. Tachiiri, K.; Abe, M.; Hajima, T.; Arakawa, O.; Suzuki, T.; Komuro, Y.; Ogochi, K.; Watanabe, M.; Yamamoto, A.; Tatebe, H. *MIROC MIROC-ES2L Model Output Prepared for CMIP6 ScenarioMIP SSP585*; Version 20190823; Earth System Grid Federation: Greenbelt, MD, USA, 2019.
32. Seland, Ø.; Bentsen, M.; Olivieri, D.J.L.; Toniazzi, T.; Gjermundsen, A.; Graff, L.S.; Debernard, J.B.; Gupta, A.K.; He, Y.; Kirkevåg, A. *NCC NorESM2-LM Model Output Prepared for CMIP6 ScenarioMIP SSP585*; Version 20200218; Earth System Grid Federation: Greenbelt, MD, USA, 2019.
33. Byun, Y.-H.; Lim, Y.-J.; Shim, S.; Sung, H.-M.; Sun, M.; Kim, J.; Kim, B.-H.; Lee, J.-H.; Moon, H. *NIMS-KMA KACE1. 0-G Model Output Prepared for CMIP6 ScenarioMIP SSP585*; Version 20200130; Earth System Grid Federation: Greenbelt, MD, USA, 2019.
34. Sung, J.H.; Eum, H.-I.; Park, J.; Cho, J. Assessment of climate change impacts on extreme precipitation events: Applications of CMIP5 climate projections statistically downscaled over South Korea. *Adv Meteorol.* **2018**, *2018*, 4720523. [[CrossRef](#)]
35. Das, J.; Nanduri, U.V. Future projection of precipitation and temperature extremes using change factor method over a river basin: Case study. *J. Hazard. Toxic Radioact. Waste* **2018**, *22*, 04018006. [[CrossRef](#)]
36. Das, J.; Manikanta, V.; Umamahesh, N.V. Population exposure to compound extreme events in India under different emission and population scenarios. *Sci. Total Environ.* **2022**, *806*, 150424. [[CrossRef](#)] [[PubMed](#)]
37. Das, J.; Umamahesh, N.V. Heat wave magnitude over India under changing climate: Projections from CMIP5 and CMIP6 experiments. *Int. J. Climatol.* **2022**, *42*, 331–351. [[CrossRef](#)]
38. Carvalho, D.; Rafael, S.; Monteiro, A.; Rodrigues, V.; Lopes, M.; Rocha, A. How well have CMIP3, CMIP5 and CMIP6 future climate projections portrayed the recently observed warming. *Sci. Rep.* **2022**, *12*, 11983. [[CrossRef](#)]

**Disclaimer/Publisher's Note:** The statements, opinions and data contained in all publications are solely those of the individual author(s) and contributor(s) and not of MDPI and/or the editor(s). MDPI and/or the editor(s) disclaim responsibility for any injury to people or property resulting from any ideas, methods, instructions or products referred to in the content.